

# The Gravitational Wave Emission of Double White Dwarf Coalescences

Ze-Cheng Zou<sup>1</sup>, Xiao-Long Zhou<sup>1</sup> and Yong-Feng Huang<sup>1,2</sup>

<sup>1</sup> School of Astronomy and Space Science, Nanjing University, Nanjing 210023, P. R. China; [hyf@nju.edu.cn](mailto:hyf@nju.edu.cn)

<sup>2</sup> Key Laboratory of Modern Astronomy and Astrophysics (Nanjing University), Ministry of Education, P. R. China

Received 20xx month day; accepted 20xx month day

**Abstract** Type Ia Supernovae (SNe Ia) are widely used as standard candles to probe the Universe. However, how these fierce explosions are produced itself is still a highly debated issue. There are mainly two popular models for SNe Ia, i.e. the double-degenerate scenario and the single-degenerate scenario. The double-degenerate scenario suggests that SNe Ia are produced by the coalescence of two degenerate white dwarfs, while the single-degenerate scenario suggests that the continuous accretion of a single degenerate white dwarf from its normal stellar companion will finally lead to a disastrous explosion when it is over-massive, resulting in an SN Ia. The rapid development of the gravitational wave astronomy sheds new light on the nature of SNe Ia. In this study, we calculate the gravitational wave emissions of double white dwarf coalescences and compare them with the sensitivities of several upcoming detectors. It is found that the gravitational wave emissions from double white dwarf mergers in the locale universe are strong enough to be detected by LISA. We argue that LISA-like gravitational wave detectors sensitive in the frequency range of 0.01 — 0.1 Hz will be a powerful tool to test the double-degenerate model of SNe Ia, and also to probe the Universe.

**Key words:** White dwarfs, Gravitational waves, Supernovae: general

## 1 INTRODUCTION

Type Ia supernovae (SNe Ia) represent a kind of high-energy astrophysical phenomena with similar light curves in the universe. Typically, the peak luminosity of SN Ia, the color at the peak time, and the decline rate of the brightness after the peak luminosity are found to follow the so-called Phillips relationship (Phillips 1993; Phillips et al. 1999; Kattner et al. 2012). This makes SNe Ia a useful tool to act as standard candles in cosmological distance measurements. They have been widely used in determining cosmological parameters. Using SNe Ia, researchers have found the acceleration of cosmic expansion (Perlmutter et al. 1999; Riess et al. 1998). However, note that the explosion mechanism of SNe Ia and their exact progenitors are still highly debated (Nomoto et al. 1997; Wang & Han 2012; Maoz et al. 2014).

In principle, SNe Ia are believed to be related to electron-degenerate matter. When an electron-degenerate star, i.e. a white dwarf (WD), accretes continuously from its companion, it will finally become more massive than the Chandrasekhar limit and the electron-degenerate pressure will not be able to balance the self-gravity. It will result in an explosive collapse and give birth to an SN Ia. Still, there are at least two popular scenarios of SNe Ia following this idea, i.e., the single-degenerate scenario and the double-degenerate scenario. In the single-degenerate scenario, a WD in a binary system accretes matter from its normal companion star. The accretion continues till the WD reaches the Chandrasekhar limit and the explosion happens (Hachisu et al. 1996; Li & van den Heuvel 1997; Han & Podsiadlowski 2004; Wang et al. 2009). In the double-degenerate scenario, two WDs form a binary system and lose their orbital energy due to gravitational wave (GW) emission. At the last stage of the inspiraling, the less massive WD is tidally disrupted and a merger event is subsequently produce. An SN Ia will occur if the merger leads to central carbon ignition (e.g., Iben & Tutukov 1984; Webbink 1984).

The single-degenerate scenario is more popular nowadays, yet it faces many serious problems (e.g., Wang 2018). For example, the details of the detonation waves and the ignition are still quite unclear (Peng 1999). Additionally, there is a lack of hydrogen in the observed spectra of SNe Ia (Livio & Mazzali 2018). The double-degenerate scenario, on the contrary, is well consistent with this spectral feature. Moreover, the existence of a significant amount of double WD systems have been directly proved by various observations (Iben & Tutukov 1984; Iben & Livio 1993; Saffer et al. 1998; Roelofs et al. 2010), and some of them have

even been found to show orbital decay as predicted by the general relativity theory so that they should definitely merge in the future (e.g., [Brown et al. 2011](#); [Hermes et al. 2012](#); [Kilic et al. 2014](#)). More interestingly, several authors recently calculated the chemical outcome of double WD collisions by means of numerical simulations. They found that their results are consistent with observed SN Ia spectra ([Kushnir et al. 2013](#); [Dong et al. 2015](#); [Isern & Bravo 2018](#)). Meanwhile, we should also note that the double-degenerate scenario also faces some serious problems. First, it has difficulties in explaining the similarities of most SNe Ia as the WD explosion mass has a relatively wide range. Second, several studies reveal that the outcome of double WD mergers may be a neutron star resulting from an accretion-induced collapse, rather than a thermonuclear explosion as required by the observed SNe Ia ([Nomoto & Iben 1985](#); [Saio & Nomoto 1998](#)). These arguments are based on the assumption that the merging remnant consists of a hot envelope or a thick disc, or even both upon the primary WD. In this case, the accreting oxygen-neon WD would finally collapse into a neutron star when it approaches the Chandrasekhar limit. Interestingly, [Pakmor et al. \(2010\)](#) proposed a new violent merger scenario for SNe Ia based on the merging of double WDs. In their scenario, a prompt detonation is triggered while the merger is still ongoing, giving rise to an SN Ia explosion. In short, the final fates (collapse to a neutron star or thermonuclear explosion as an SN Ia) of double WD mergers are strongly dependent on the merging processes (e.g. slow merger, fast merger, composite merger, violent merger, etc).

While the trigger mechanism of SNe Ia is still quite unclear, the rapid development of GW astronomy could shed new light on their nature. In the double-degenerate scenario, a strong GW emission is expected as the two degenerate WD stars spiral in before the final merging. Decihertz interferometers such as the DECIGO and B-DECIGO ([Isoyama et al. 2018](#); [Sato et al. 2017](#); [Yagi & Seto 2011](#)) can detect the most massive binary WDs in our Galaxy ([Maselli et al. 2019](#)), and less massive binary WDs may be targets for detectors working in millihertz regime like LISA. On the contrary, in the single-degenerate scenario, GW emission should be weak during the whole process.

In this study, we investigate the last stage of double WDs' inspiraling and their GW emissions. We simulate the evolution of the GW signals and obtain the spectra features. Especially, we examine whether LISA can detect the GW signature if SNe Ia are produced by double-degenerate star mergers. The structure of our paper is organized as follows. In Sect. 2, we describe the strain amplitude of GW from double WD systems. In Sect. 3, the observable quantity of strain spectral amplitude is introduced. In Sect. 4, the cut-off frequency of the gravitational wave from a merging double WD system is calculated and compared with the spectral range of GW detectors. In Sect. 5, we calculate the GW emission produced by some recent SNe Ia in framework of the double-degenerate scenario, and confront the results with GW detectors. Finally, our conclusions and discussion are presented in Sect. 6.

## 2 GRAVITATIONAL WAVE STRAIN AMPLITUDE

In this study, we consider a binary system consisting of two WDs with equal mass  $M$  rotating in a circular orbit around the common barycentre. It has been argued that in the double-degenerate scenario, the mass ratio (defined as the mass of the less massive WD divided by the mass of its more massive companion) of the two WDs should be larger than 0.8 to ignite an SN Ia ([Pakmor et al. 2011](#)). So, the equal-mass assumption is acceptable in considering the GW emission from the system. Since the separation between the two WDs is still relatively large even at the final stage that they are disrupted by tidal force, Newtonian mechanics is roughly applicable for the orbital motion during the whole inspiraling process. According to Kepler's law, the orbit frequency is

$$f_{orb} = \sqrt{\frac{GM}{2\pi^2 R^3}}, \quad (1)$$

where  $R$  is the separation between the two stars and  $G$  is the gravitational constant. Correspondingly, the frequency of GW is

$$f = 2f_{orb} = \sqrt{\frac{2GM}{\pi^2 R^3}}. \quad (2)$$

The GW power emitted by the binary can be calculated by the following formula

$$P = \frac{64G^4 M^5}{5c^5 R^5}, \quad (3)$$

where  $c$  is the velocity of light.

As the double WD system emitting GW at the aforementioned power, the frequency of GW will gradually decline as ([Creighton & Anderson 2011](#))

$$\dot{f} = \frac{96}{5} \frac{c^3}{G} \frac{f}{M_c} \left( \frac{G}{c^3} \pi f M_c \right)^{8/3}, \quad (4)$$

due to the energy loss, where  $M_c$  is the chirp mass defined as

$$M_c = \frac{(m_1 m_2)^{3/5}}{(m_1 + m_2)^{1/5}}. \quad (5)$$

The GW can have two polarization states, with the amplitude usually designated as  $h_+$  and  $h_\times$ , respectively (Landau & Lifshitz 2012; Postnov & Yungelson 2014). The overall GW amplitude is then

$$h = \sqrt{(h_+)^2 + (h_\times)^2}. \quad (6)$$

After averaging the gravitational wave signal in whole period, the amplitude is

$$h = \left(\frac{32}{5}\right)^2 \frac{G}{c^2} \frac{M_c}{d} \left(\frac{G}{c^3} \pi f M_c\right)^{2/3}, \quad (7)$$

where  $d$  is the distance of the GW source with respect to us (Postnov & Yungelson 2014).

### 3 GRAVITATIONAL WAVE STRAIN SPECTRAL AMPLITUDE

In studying the detectability of GWs, it is more important to consider the signal-to-noise ratio (SNR), i.e., whether the effect of GWs is higher than the sensitivity of the detector (Robson et al. 2019; Wong et al. 2018). In the inspiraling phase, the energy density of GW (Postnov & Yungelson 2014) can be expressed as

$$S_h = \frac{G^{5/3}}{c^3} \frac{\pi}{12} \frac{M_c^{5/3}}{d^2} \frac{1}{(\pi f)^{7/3}}. \quad (8)$$

The strain spectral amplitude ( $h_f$ ) is the Fourier transformation of  $h$ . In the inspiraling phase of a binary WD system, the frequency generally evolves very slowly, so that the strain spectral amplitude can be expressed as (Postnov & Yungelson 2014; Geng et al. 2015; Robson et al. 2019),

$$h_f = \sqrt{S_h} = \sqrt{\frac{G^{5/3}}{c^3} \frac{\pi}{12} \frac{M_c^{5/3}}{d^2} \frac{1}{(\pi f)^{7/3}}}. \quad (9)$$

This equation is applicable mainly at the late stage of the inspiraling process. It is accurate enough even at the moment when the less massive WD is to be disrupted by its companion.

However, note that at the early stage of the inspiraling, the two WDs are far from each other and the variation rate of the GW frequency is extremely small, i.e.  $\dot{f} \times T_{obs} < 1/T_{obs}$ , where  $T_{obs}$  is integration time for a continuous observation. It means that the emitted GW is nearly monochromatic and the observed GW frequency almost does not change during the observation period of  $T_{obs}$ . As a result, it is the integration time that restricts the observed SNR and the above expression of  $h_f$  is inappropriate. For a particular integration time  $T_{obs}$ , to determine when the expression of  $h_f$  (i.e. Eq. 9) begins to be applicable, we can set  $\dot{f} \times T_{obs} = 1/T_{obs}$  and derive the corresponding GW frequency as

$$f_T = \left(\frac{8}{3} \frac{\kappa}{T_{obs}^2}\right)^{3/11}, \quad (10)$$

where  $\kappa$  is defined as

$$\kappa = \frac{5}{256} \left(\frac{G}{c^3} M_c\right)^{-5/3} \pi^{-8/3}. \quad (11)$$

When  $f > f_T$ , the evolution of the GW frequency becomes significant and the sensitivity are determined by Eq. 9. In our study, we take the integration time as 4 years for all the following numerical calculations. This is the planned duty time of LISA L3 mission (Amaro-Seoane et al. 2017).

### 4 CUT-OFF FREQUENCY OF THE GRAVITATIONAL WAVE

The inspiraling is a gradual process. With the gradual decrease of the orbital separation, the GW frequency increases correspondingly. As a result, according to Eqs. 7 and 9, the strain amplitude of GW increases while the strain spectral amplitude decreases gradually. Finally, the GW emission will be ceased when the less massive WD is tidally disrupted by its companion. This happens at the so called tidal disruption radius (Hills 1975), when the separation between the two WDs is

$$R_{td} \approx \left(\frac{6M}{\pi\rho}\right)^{1/3}, \quad (12)$$

where  $\rho$  is the mean density of the less massive white dwarf. Taken  $\rho = 10^9 \text{ kg m}^{-3}$ , we get  $R_{td} \approx 1.56 \times 10^7 (M/M_\odot)^{1/3} \text{ m}$ . At this separation, the gravity is  $1.08 \times 10^{37} (M/M_\odot)^{4/3} \text{ N}$ . It means that the gravity is not too strong and the Newtonian mechanical assumption is applicable.

Just before the tidal disruption separation, the GW emission power comes to a maximum and the GW frequency is also the highest. After being tidally disrupted, the GW emission will be almost completely cut-off. Combining Eqs. 2 and 12, the cut-off frequency can be derived as

$$f_{cut} = \sqrt{\frac{G}{3\pi}} \rho. \quad (13)$$

A rough estimation shows that the cut-off frequency of GW from binary WDs are around 1 Hz. Especially, at this last stage, the variation rate of the GW frequency is around  $10^{-5} \text{ s}^{-2}$ . We see that this rate is actually small enough so that the applicability of Eq. 9 is guaranteed.

## 5 NUMERICAL RESULTS

According to Eqs. 7 and 9, the strain amplitude and the strain spectral amplitude of GWs are mainly determined by the masses of the WDs. In this study, for simplicity, we assume that the two companion WDs are equal in mass. As an exemplar investigation, we take three typical values for the WD mass in our calculations, i.e.  $0.5 M_\odot$ ,  $0.8 M_\odot$ , and  $1.0 M_\odot$ . Note that the  $0.5 M_\odot$ -WD binary mergers in fact are unlikely lead to SNe Ia. In the violent merger scenario, a detonation leading to an SN Ia explosion in the merger phase may not be triggered for double WDs with individual mass lower than  $0.8 M_\odot$  (Sim et al. 2010). Moreover, Sato et al. (2015) also argued that for the primary WD of  $0.7 M_\odot < M < 0.9 M_\odot$ , a total mass larger than  $1.38 M_\odot$  is required to trigger an SN Ia detonation in the stationary rotating merger remnant phase. However, since low-mass WDs are very common (see Fig. 1) and low-mass binary WDs form the most numerous population among all binary WDs (Postnov & Yungelson 2014), we use the  $0.5 M_\odot$  case as a representation of these interesting low mass WD binaries. In fact, they are important goals of many GW experiments.

At the same time, we notice that the cut-off frequency of the GW emission mainly depends on the density of WDs (see Eq. 13). In order to calculate the GW evolution of binary WDs of certain masses, we need to know the relationship between density and mass of WDs. For this purpose, we mainly resort to the observational data of WDs. The Montreal White Dwarf Database (MWDD) provides a useful data source, which lists the observed parameters for WDs (Dufour et al. 2017, <http://montrealwhitedwarfdatabase.org/>), including the mass and radius for a significant portion of them so that the mean density can be derived. Using the MWDD data, we have plotted in Fig. 1 the density versus mass for all the observed WDs with data available.

Inside a WD, the gravity is balanced mainly by the pressure of degenerate electrons. So the mass-radius relation of WDs can be conveniently derived by theoretical analysis. A simple dimensional analysis gives that the radius of a WD with mass  $M$  scales as  $r \propto \mu_e^{-5/3} M^{-1/3}$ , where  $\mu_e$  is the average baryon number per electron (Koester & Chanmugam 1990). In fact, in the non-relativistic case, the detailed mass-radius relation has been derived by Chandrasekhar (1935) as,

$$r \approx 2.785 \times 10^9 \text{ cm} \times (M/1M_\odot)^{-1/3} \mu_e^{-5/3}. \quad (14)$$

Note that Eq. 14 is applicable mainly for low mass WDs, which have relatively larger radii so that the gravity on the WD surface is not too strong. For higher mass WDs, the relativistic effect should be taken into consideration. In this case, the equilibrium equations become much more complicated and could only be numerically solved. Numerical results on relativistic WDs have also been obtained and provided as a data table by Chandrasekhar (1967). To present a direct comparison with observations, we have plotted the theoretical mass-density relations of WDs in Fig. 1. The dashed curve is the non-relativistic relation calculated from Eq. 14, taking  $\mu_e = 2$ , and the solid curve corresponds to the relativistic relation as presented in the data table of Chandrasekhar (1967). We see that the non-relativistic curve matches well with the observational data points in the low mass segment, while the relativistic curve is consistent with the data points even at the high mass end. However, we should also note that the observational data points are generally quite scattered as compared with the theoretical curve, which means WDs of a particular mass can have very different radii. This may be caused by their different internal composition. Also, the crust may play an important role on the WD radius.

From Fig. 1, we can clearly see that more massive WDs tend to have a higher mean density. The observed data points could provide a reliable clue on the WD density. Especially, we see that when the WD mass is  $0.5 M_\odot$ ,  $0.8 M_\odot$ , or  $1.0 M_\odot$ , the corresponding mean density is typically  $10^8 \text{ kg m}^{-3}$ ,  $10^9 \text{ kg m}^{-3}$ , and  $3 \times 10^9 \text{ kg m}^{-3}$ . With the hints from Fig. 1, we finally take the following three typical mass-density pairs in our subsequent calculations:  $m_1 = 0.5 M_\odot$ ,  $\rho_1 = 10^8 \text{ kg m}^{-3}$ ;  $m_2 = 0.8 M_\odot$ ,  $\rho_2 = 10^9 \text{ kg m}^{-3}$ ;  $m_3 = 1.0 M_\odot$ ,  $\rho_3 = 3 \times 10^9 \text{ kg m}^{-3}$ .

Using the aforementioned typical parameters, we have simulated the dynamical evolution of the inspiraling process of various double WD systems. In our calculations, we follow the inspiraling process till the two WDs come to the tidal disruption radius so that the GW emission essentially ceases. Fig. 2 illustrates the GW frequency versus time for the three cases. It can be clearly seen that at the final stage, the GW frequency is typically in a range of 0.01 — 0.1 Hz. It is undetectable for LIGO and Einstein Telescope (which operate for GWs ranging from hertz to kilohertz), but is well within the sensitive range of the future LISA experiment (from millihertz to hertz). These GW events may also be targets of the B-DECIGO

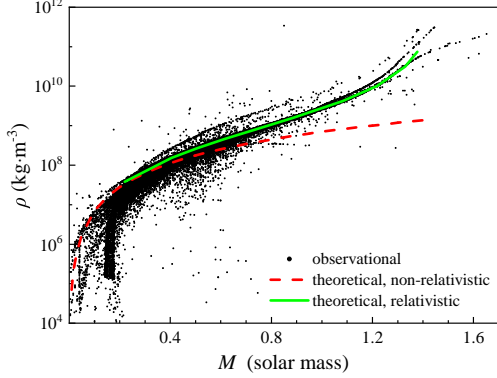


Fig. 1: Mean density versus mass for the currently observed WDs. Each point represents a WD. The observational data are taken from the Montreal White Dwarf Database (Dufour et al. 2017). The mean density is calculated from the observed mass and the surface gravitational acceleration, assuming a spherical configuration without spinning. The dashed curve and the solid curve represent theoretical non-relativistic (Chandrasekhar 1935) and relativistic (Chandrasekhar 1967) mass-density relations of WDs, respectively.

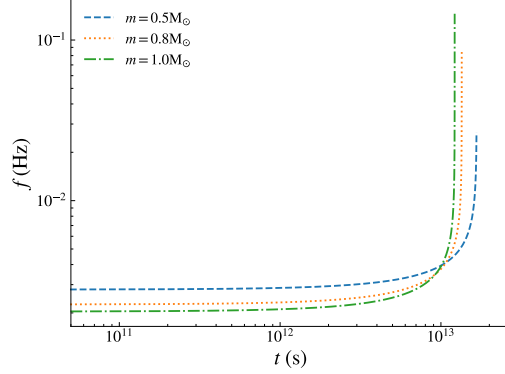


Fig. 2: Evolution of the GW frequency for a double WD system. The orbit is assumed to be circular throughout the inspiraling process.  $t = 0$  corresponds to the moment that the GW frequency equals to  $f_T$ . The dashed, dotted, and dash-dotted lines correspond to a WD mass of  $0.5M_\odot$ ,  $0.8M_\odot$  and  $1.0M_\odot$ , respectively. For each curve, the highest frequency corresponds to the cut-off frequency when the WDs are tidally disrupted.

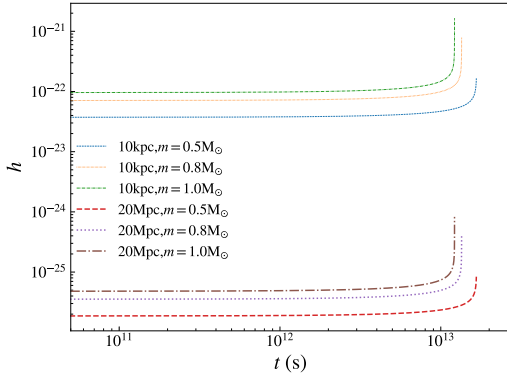


Fig. 3: Evolution of the GW strain amplitude for double WD systems. The parameters are the same as in Fig. 2. The thin dashed, dotted, and dash-dotted lines corresponds to a WD mass of  $0.5M_\odot$ ,  $0.8M_\odot$ , and  $1.0M_\odot$ , respectively, at a distance of 10 kpc. For the thick lines, the distance is taken as 20 Mpc while other parameters remain unchanged.

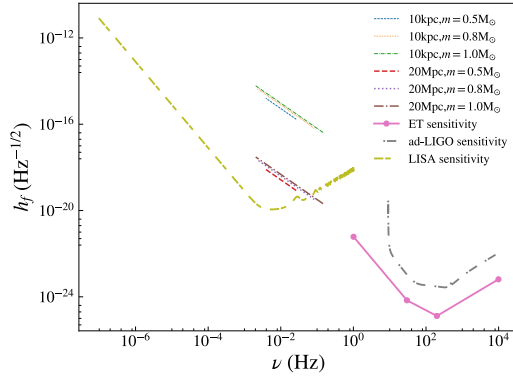


Fig. 4: Evolution of the GW strain spectral amplitude for double WD systems. The parameters and line styles are the same as in Fig. 3. As a comparison, the sensitivity curves of Einstein Telescope (the thick solid curve; Hild et al. 2008), advanced LIGO (the thick dash-dotted curve; Harry 2010), and LISA (the thick double-dashed curve; Larson et al. 2000) are also plotted.

detector, as suggested by Maselli et al. (2019). Also, we see that when the WD mass is larger, the cut-off frequency is also significantly higher. This is because for a high-mass WD, the mean density is also relatively high. Then according to Eq. 12, the WD will be disrupted at a smaller radius, and the cut-off frequency is correspondingly higher as indicated by Eq. 13.

In Fig. 3, we illustrate the evolution of the GW strain amplitude for double WD systems. In this plot, we assume two different luminosity distances for the GW sources, 10 kpc and 20 Mpc. Again we see that the GW strain amplitude is markedly enhanced when the WD mass increases. When the WD mass varies from  $0.5 M_\odot$  to  $1.0 M_\odot$  and increases by a factor of only two, the strain amplitude increases by a factor of about 10. In the 10 kpc distance cases, the strain amplitude can be as high as  $10^{-22}$  —  $10^{-21}$  at the final stage. The amplitude is in the range of  $10^{-25}$  —  $10^{-24}$  even in the 20 Mpc cases.

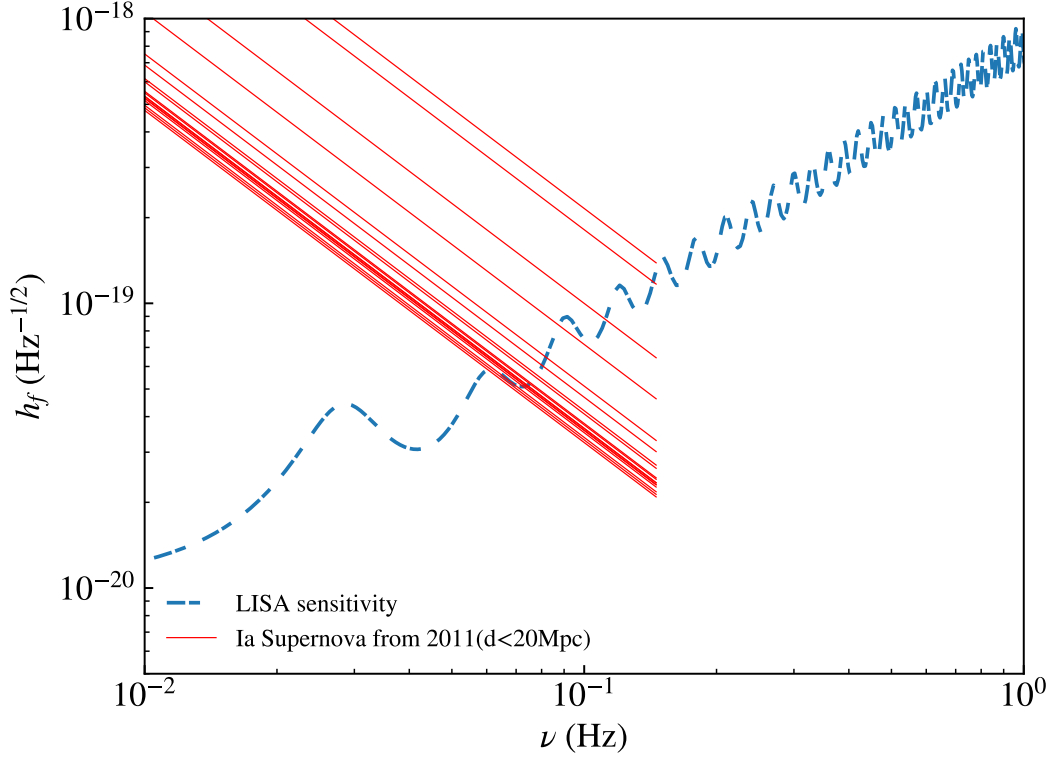


Fig. 5: Simulated GW strain spectral amplitude for some observed SNe Ia in the framework of the double-degenerate scenario. Each SN Ia is represented by a solid straight line. The dashed curve represents the sensitivity curve of LISA.

In order to know whether the GW is strong enough to be detected by GW instruments, we need to compare the strain spectral amplitude with the sensitivities of the detectors. In Fig. 4, we have plotted the strain spectra amplitude of different WD binary systems, together with the sensitivity curves of LISA, advanced LIGO and Einstein Telescope. We see that GW emissions from double WD systems are not in the sensitive frequency ranges of advanced LIGO and Einstein Telescope, but are satisfactory targets for LISA. LISA can detect the GW of the binary WDs in our Milky Way Galaxy at a very high SNR (represented by the 10-kpc cases). More encouragingly, it can also detect such events in our local Universe to a distance much larger than 20 Mpc.

Many SNe Ia have been observed till now. They are widely used in cosmology researches. If SNe Ia are produced via the double-degenerate mechanism, then the associated GW emissions should be detectable to LISA and the trigger mechanism can be firmly tested. The Open Supernova Catalog (Guillochon et al. 2017, <https://sne.space/>) provides a complete list of SNe Ia observed so far. Using this data base, we have selected all the SNe Ia discovered since 2011, with the luminosity distance smaller than 20 Mpc. There are 19 events satisfying this criterion. We assume that all these SNe Ia were produced via the double-degenerate mechanism. For simplicity, the masses of the WDs are taken as  $1.0 M_{\odot}$  for all of them. In Fig. 5, the strain spectral amplitudes expected from these 19 events are plotted and compared with the sensitivity curve of LISA. Encouragingly, we see that all these events are detectable to LISA even in the earlier inspiraling stage. We thus argue that LISA will be a powerful tool to test the double-degenerate mechanism for SNe Ia.

## 6 CONCLUSIONS AND DISCUSSIONS

Whether SNe Ia are produced by the single-degenerate mechanism or the double-degenerate mechanism is still a highly debated issue. In this study, we investigate the GW emissions from inspiraling double WD systems. Different from merging double black holes or double neutron stars (e.g. Abbott et al. 2016, 2017), merging double WD systems cannot be detected by ground-based GW detectors such as the Advanced LIGO or the future Einstein Telescope. However, they are appropriate targets for space-based interferometers like LISA or Taiji (Ruan et al. 2019). Especially, it is found that LISA can essentially detect the GW emission from almost all SNe Ia within a distance of 20 Mpc if they are triggered by the double-degenerate mechanism. As a result, LISA will be a powerful tool to examine the trigger mechanism of SNe Ia.

Many double WD binaries have been discovered in our Galaxy. Thus the merging of binary WDs will undoubtedly happen in our local Universe. Considering that the actual detecting distance of LISA can be

significantly larger than 20 Mpc, we believe that LISA will be able to detect plenty of merging WDs in the future. It is interesting to note that the luminosity distances of these chirping GW sources can be directly measured through GW observations themselves (Schutz 1986; Messenger & Read 2012). Additionally, the masses of each WD can also be measured. It is expected that LISA observations of future SNe Ia will not only help to examine the double-degenerate model of SNe Ia, but also provide valuable information on the distances so that SNe Ia could act as more precise standard candles.

Traditionally, SNe Ia could only be studied based on multi-wavelength electro-magnetic observations (Tutukov & Fedorova 2007), assisted by some theoretical calculations on the chemical outcome during the bursting process (e.g. Liu et al. 2018; Isern & Bravo 2018). As a result, it is hard to draw any firm conclusions on the progenitors. Gravitational wave can work as a completely new messenger for understanding the nature of SNe Ia. LISA can hopefully help make firm constraints on this issue. It may lead the cosmology study into a new era (Wang et al. 2003). If the double-degenerate scenario was found correct, or the mechanism contributed at least a fraction of SNe Ia, then previous cosmology results based on the single-degenerate scenario would be markedly modified.

**Acknowledgements** We acknowledge the anonymous referee for valuable suggestions that lead to an overall improvement of this study. We thank Jinjun Geng for useful discussion and help. This work was supported by the National Natural Science Foundation of China (Grant No. 11873030), and by the Strategic Priority Research Program of the Chinese Academy of Sciences (“multi-waveband Gravitational Wave Universe”, Grant No. XDB23040000).

## References

- Abbott, B. P., Abbott, R., Abbott, T. D., et al. 2016, *Phys. Rev. Lett.*, 116, 061102 [6](#)  
 Abbott, B. P., Abbott, R., Abbott, T. D., et al. 2017, *Phys. Rev. Lett.*, 119, 161101 [6](#)  
 Amaro-Seoane, P., Audley, H., Babak, S., et al. 2017, arXiv:1702.00786 [3](#)  
 Brown, W. R., Kilic, M., Hermes, J. J., et al. 2011, *ApJL*, 737, L23 [2](#)  
 Chandrasekhar, S. 1935, *MNRAS*, 95, 207 [4, 5](#)  
 Chandrasekhar, S. 1967, *An Introduction to the Study of Stellar Structure* (Dover Publications, New York) [4, 5](#)  
 Creighton, J. D. E., & Anderson, W. G. 2011, *Gravitational-Wave Physics and Astronomy* (Wiley-VCH, Singapore) [2](#)  
 Dong, S., Katz, B., Kushner, D., & Prieto, J. L. 2015, *MNRAS*, 454, L61 [2](#)  
 Dufour, P., Blouin, S., Coutu, S., et al. 2017, 20th European Workshop on White Dwarfs (EuroWD16), ed. P.-E. Tremblay, B. Gnsicke, & T. Marsh (Astronomical Society of the Pacific, San Francisco), 3 [4, 5](#)  
 Geng, J. J., Huang, Y. F., & Lu, T. 2015, *ApJ*, 804, 21 [3](#)  
 Guillochon, J., Parrent, J., Kelley, L. Z., & Margutti, R. 2017, *ApJ*, 835, 64 [6](#)  
 Hachisu, I., Kato, M., & Nomoto, K. 1996, *ApJL*, 470, L97 [1](#)  
 Han, Z., & Podsiadlowski, Ph. 2004, *MNRAS*, 350, 1301 [1](#)  
 Harry, G. M. 2010, *Class. Quantum Grav.*, 27, 084006 [5](#)  
 Hermes, J. J., Kilic, M., Brown W. R., et al. 2012, *ApJL*, 757, L21 [2](#)  
 Hild, S., Chelkowski, S., & Freise, A. 2008, arXiv:0810.0604 [5](#)  
 Hills, J. G. 1975, *Nature*, 254, 295 [3](#)  
 Iben, I. Jr, & Livio, M. 1993, *PASP*, 105, 1373 [1](#)  
 Iben, I. Jr, & Tutukov, A. 1984, *ApJS*, 55, 335 [1](#)  
 Isern, J., & Bravo, E. 2018, *Res. Notes AAS*, 2, 157 [2, 7](#)  
 Isoyama, S., Nakano, H., & Nakamura, T. 2018, *PTEP*, 2018, 073E01 [2](#)  
 Kattner, S., Leonard, D. C., Burns, C. R., et al. 2012, *PASP*, 124, 114 [1](#)  
 Kilic, M., Brown, W. R., Gianninas, A., et al. 2014, *MNRAS*, 444, L1 [2](#)  
 Koester, D., & Chanmugam, G. 1990, *Rep. Prog. Phys.*, 53, 837 [4](#)  
 Kushnir, D., Katz, B., Dong, S., Livne, E., & Fernández, R. 2013, *ApJL*, 778, L37 [2](#)  
 Landau, L. D. & Lifshitz, E. M. 2012, *The Classical Theory of Fields* (Higher Education Press, Beijing) [3](#)  
 Larson, S. L., Hiscock, W. A., & Hellings, R. W. 2000, *Phys. Rev. D*, 62, 062001 [5](#)  
 Li, X. -D., & van den Heuvel, E. P. J. 1997, *A&A*, 322, L9 [1](#)  
 Liu, D., Wang, B., & Han, Z. 2018, *MNRAS*, 473, 5352 [7](#)  
 Livio, M., & Mazzali, P. 2018, *Phys. Rep.*, 736, 1 [1](#)  
 Maoz, D., Mannucci, F., & Nelemans, G. 2014, *ARA&A*, 52, 107 [1](#)  
 Maselli, A., Marassi, S., & Branchesi, M. 2019, arXiv:1910.00016 [astro-ph.HE] [2, 5](#)  
 Messenger, C., & Read, J. 2012, *Phys. Rev. Lett.*, 108, 091101 [7](#)  
 Nomoto, K., & Iben, I., Jr. 1985, *ApJ*, 297, 531 [2](#)  
 Nomoto, K., Iwamoto, K., & Kishimoto, N. 1997, *Science*, 276, 1378 [1](#)  
 Pakmor, R., Kromer, M., Röpke, F. K., et al. 2010, *Nature*, 463, 61 [2](#)  
 Pakmor, R., Hachinger, S., Röpke, F. K., & Hillebrandt, W. 2011, *A&A*, 528, A117 [2](#)  
 Peng, Q. 1998, *Progress in Astronomy*, 16, 60 [1](#)  
 Perlmutter, S., Aldering, G., Goldhaber, et al. 1999, *ApJ*, 517, 565 [1](#)  
 Phillips, M. M. 1993, *ApJL*, 413, L105 [1](#)  
 Phillips, M.M., Lira, P., Suntzeff, N. B., et al. 1999, *AJ*, 118, 1766 [1](#)  
 Postnov, K. A., & Yungelson, L. R. 2014, *Living Rev. Relativ.*, 17, 3 [3, 4](#)  
 Riess, A. G., Filippenko, A. V., Challis, P., et al. 1998, *AJ*, 116, 1009 [1](#)

- Robson, T., Cornish, N. J., & Liu, C. 2019, *Class. Quantum Grav.*, 36, 105011 [3](#)
- Roelofs, G. H., Rau, A., Marsh, T. R., et al. 2010, *ApJL*, 711, L138 [1](#)
- Ruan, W.-H., Guo, Z.-K., Cai, R.-G., & Zhang, Y.-Z. 2019, arXiv:1807.09495v2 [gr-qc] [6](#)
- Saffer, R. A., Livio, M., & Yungelson, L. R. 1998, *ApJ*, 502, 394 [1](#)
- Saio, H., Nomoto, K. 1998, *ApJ*, 500, 388 [2](#)
- Sato, S., Kawamura, S., Ando, M., et al. 2017, *J. Phys.: Conf. Ser.*, 840, 012010 [2](#)
- Sato, Y., NakaSato, N., Tanikawa, A., et al. 2015, *ApJ*, 807, 105 [4](#)
- Schutz, B. F. 1986, *Nature*, 323, 310 [7](#)
- Sim, S. A.; Röpke, F. K.; Hillebrandt, W., et al. 2010, *ApJL*, 714, L52 [4](#)
- Tutukov, A. V., & Fedorova, A. V. 2007, *Astron. Rep.*, 51, 291 [7](#)
- Wang, B. 2018, *RAA*, 18, 49 [1](#)
- Wang, B., & Han, Z. 2012, *NewAR*, 56, 122 [1](#)
- Wang, B., Meng, X., Chen, X., & Han, Z. 2009, *MNRAS*, 395, 847 [1](#)
- Wang, X., Li, Z., & Chen, L. 2003, *Progress in Astronomy*, 21, 55 [7](#)
- Webbink, R. F. 1984, *ApJ*, 277, 355 [1](#)
- Wong, K. W. K., Berti, E., Gabella, W. E., & Holley-Bockelmann, K. 2018, *MNRAS*, 483, L33 [3](#)
- Yagi, K., & Seto, N. 2011, *Phys. Rev. D*, 83, 044011 [2](#)